JOURNAL OF APPLIED CRYSTALLOGRAPHY

Supporting information for article:

(U)SAXS characterization of porous microstructure of chert: insights into organic matter preservation

Patricio Munoz, Jan Ilavsky, Matthew Newville, Niklaus U. Wetter, Rafael André Lourenço, Marcelo Barbosa de Andrade, Tereza S. Martins, Jessica Dipold, Anderson Z. Freitas, Luis Carlos Cides da Silva and Cristiano Luis Pinto Oliveira

S1. Wide-angle X-ray scattering profiles for combusted and intact samples

Figure S1 shows WAXS profiles collected from the intact and combusted fragments of sample S52. Tables in Figure S1 included values calculated for d-spacing, peak location on the 2θ scale, and width on the 2θ scale (integral breadth).

The integral breadth (IB) corresponds to the $(IB = \frac{[peak\ Total\ Area]}{[peak\ Heigth]})$ ratio. Total area and height were calculated using WAXS fit tool (*Irena*) and *Origin©*. The Scherrer equation (Patterson, 1939) holds:

$$D = \frac{10\ (K_{sh}\ \lambda)}{(IB\ cos\theta)}$$

Where D stands for crystallite size (in nm), K_{sh} for the Scherrer constant, λ for the radiation wavelength of used in WAXS experiments ($\lambda \sim 0.590401$ Å), and θ corresponds to the half of 2θ– positions calculated in the fitting procedure. IB is expressed in radians.

We selected some criteria to apply this formula: (1) use *IB* as an estimation of peak width, (2) a suitable K_{sh} value because our particle grains are far from isometric shapes, and (3) to calculate an average crystallite size using peak yielding non-highly variable integral breath values.

The K_{sh} is defined as the ratio between the true and apparent crystallite size in a direction perpendicular to the diffracting plane (Vargas *et al*., 1983). Highly symmetrical particles exhibit K_{sh} values around ~1 (0.89 to 0.94). However, bidimensional minerals have K_{sh} values around 0.5 to 0.7 (Drits *et al*., 1997).

Quartz and its polymorphs belong to the hexagonal and trigonal crystal systems. Thus, K_{sh} values for these mineral phases vary from 0.63 to 1.59 (Lele & Anantharaman, 1966). For hexagonal crystallites, K_{sh} generally decreases for more elongated (prolate) shapes (Lele & Anantharaman, 1966; Vargas *et al*., 1983). Thus, considering the variability reported by Lele & Anantharaman (1966), we used a minimum average value of $K_{sh} \sim 0.71$.
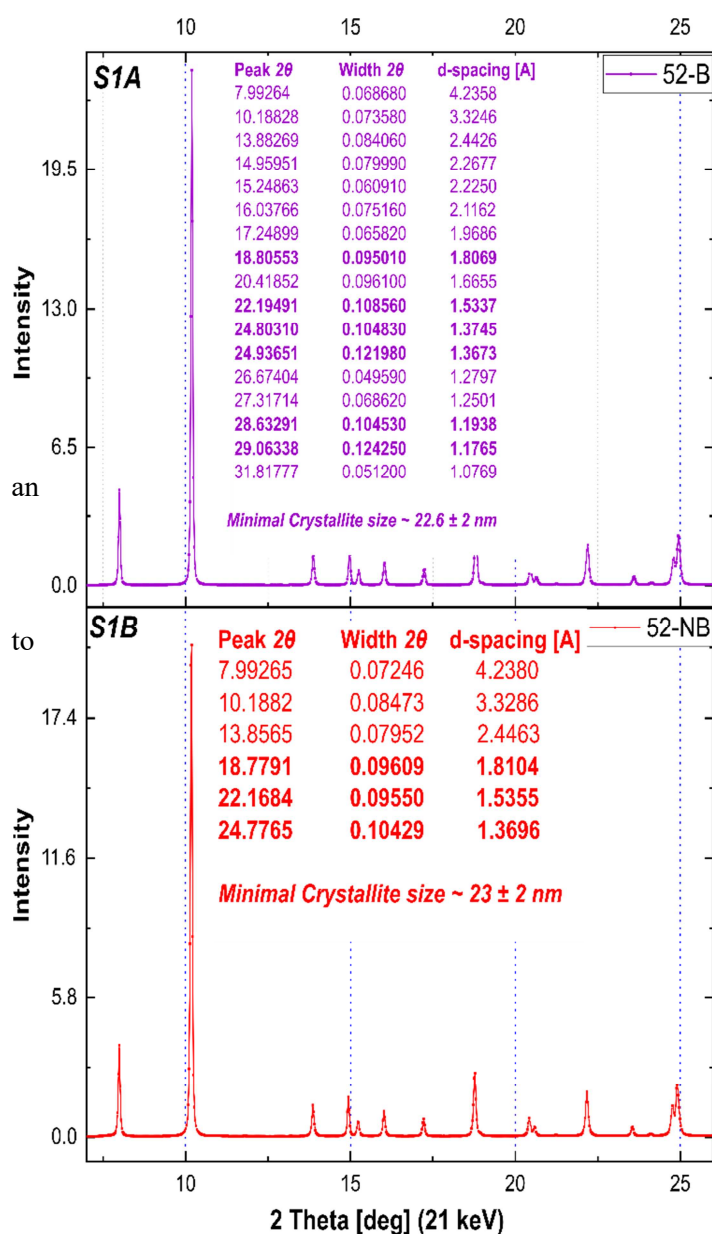
Figure S1 Comparative between intact and combusted fragment from sample S52. Combustion carried out at *UNIFESP*. WAXS experiments were performed at 9-ID beamline, *APS*, using energy beam of 21 *keV*. Combustion induced minor changes in crystallite sizes. Standard deviation was calculated the 1σ statistical significance.

S2. X-ray Microfluorescence maps (μXRF)

Figures S2.A and S2.B display the spatial distribution for some chemical elements in intact fragments (S2.A: Si, Fe, Ca; S2.B: Zn, Mn, Sr). In both samples, silicon is homogeneously distributed yielding, the highest normalized intensity regarding all other elements. But it seems to display more granular clusters in sample S1.

In sample S52, calcium spatially coincides with those displayed by Sr in granular clusters, which possibly represent micrometric carbonate grains. Additionally, iron clusters match those shown by Mn, possibly indicating tiny oxide grains. In these Fe-Mn clusters, the absence of a peak indicative of S confirms this latter interpretation.

In sample S1, Fe exhibits a homogenous spatial distribution. Some minor Fe-clusters occur at the right border of Figure S2.A(B). Possibly, most iron is distributed in sub-micrometrical grains. XRF spectra display no evidence of sulfur occurrence into these Fe-homogenous regions ruling out sulfide phases.

Finally, red grains in Figure S2.B highlight Zn-rich grains. XRF spectra indicate that some of these grains present high Ca concentrations suggesting the presence of Zn-bearing carbonates. These particular types of carbonates indicate hydrothermal effects on samples (Jacquat *et al.*, 2011).
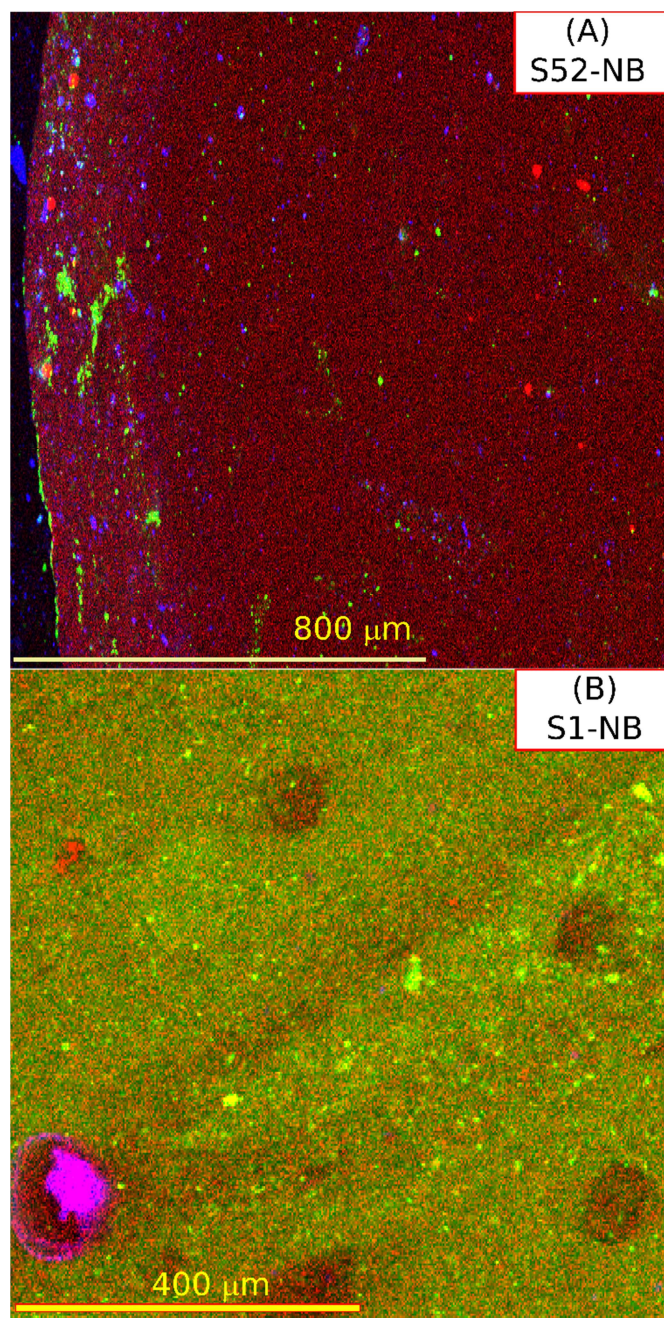
Figure S2.A Chemical maps for Si (red), Fe (green), and Ca (blue) for intact samples. Lower bars indicate the size of the scanned area. In Figure (B) spherical structure corresponds to a radiolarian microfossil (in the lower left corner). Radiolarian form silica-rich external exoskeletons uptaking silicon from sea waters.
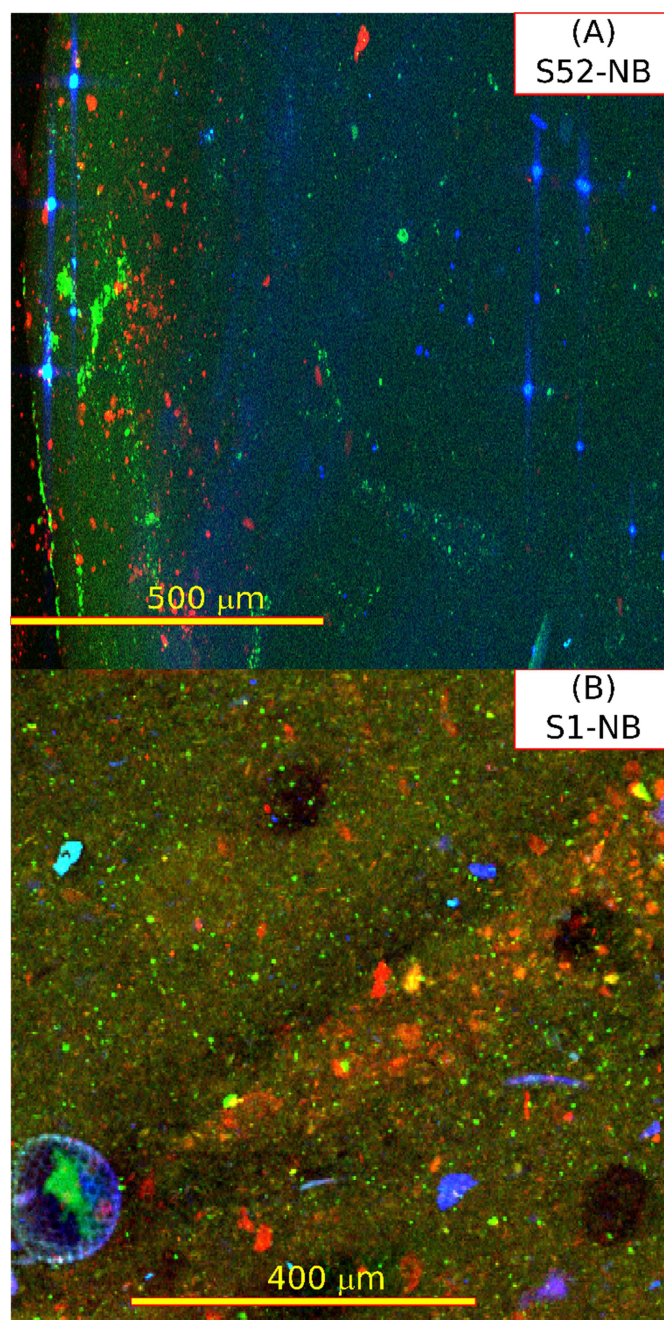
Figure S2.B Chemical map for Zn (red), Mn (green), and Sr (blue) for intact samples. Lower bars indicate the size of the scanned area.
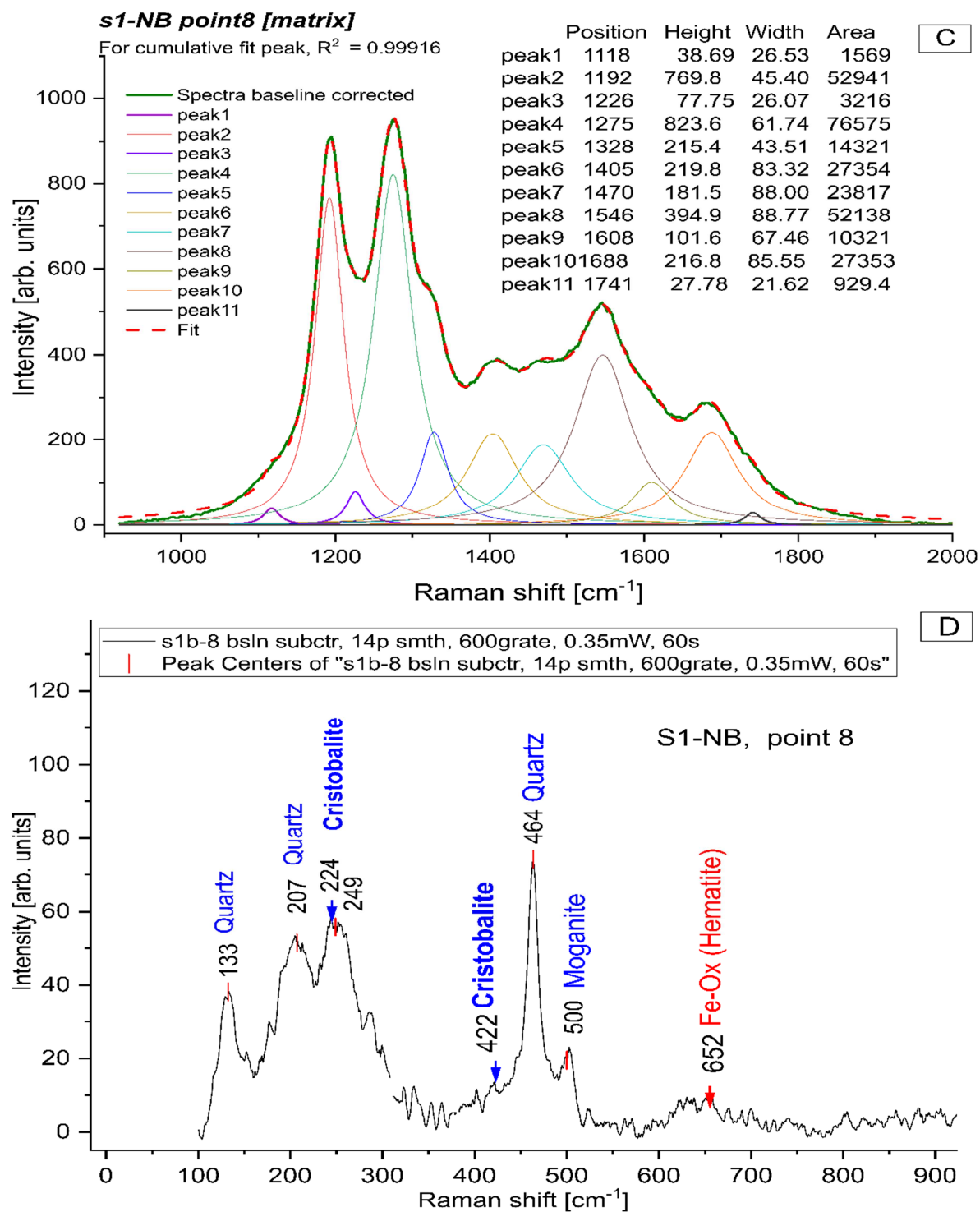
S3. Raman microspectroscopy spectra

Figures S3.1 and S3.2 show representative Raman spectra collected in intact samples. See in text discussion about spectral features representative for SiO_2 polymorphs, Fe-Ox, and bands for graphite (carbonaceous OM in samples S52 and S51; Figures A and B). In sample S1, an initial peak fingerprint indicates occurrence of some organics (Figure D): (1) peaks at 1118 cm^{-1}, 1275 cm^{-1} and 1546 cm^{-1} possibly represent scytonemin (bacterial pigment), (2) peak at 1226 cm^{-1} could represent riboflavin, (3) peak at 1405 cm^{-1} represents pyrene (PAHs), and (4) peak at 1608 cm^{-1} could represents phenylalanine. A more detailed fingerprint will be addressed in future research.

Post-background corrections intensities for bands D (I_D) and G (I_G) were used as input for the calculation of aromatic cluster sizes (Figures A and B, S3A).
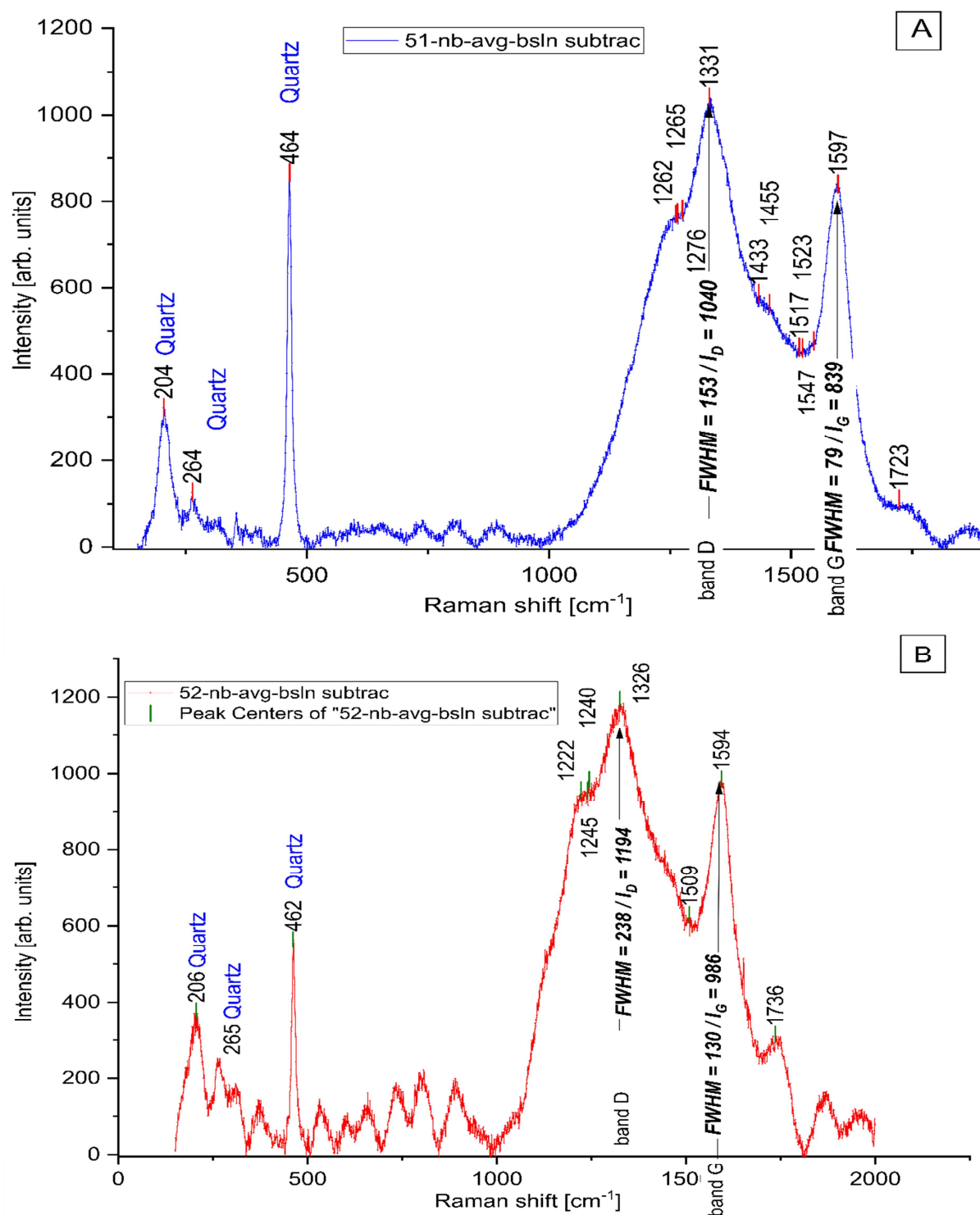
Figure S3.1 Representative Raman spectra for intact samples S51 (A), S52 (B). Peaks were identified by deconvolution using Lorentzian peaks in spectra for samples S51 and S52 (Origin©). Data were collected at *IPEN-CNEN* using wavelength of 785 nm, objective of 50x, acquisition time of some seconds, power ~ 100mW, and a beam diameter of ~ 1.3 μm.

s1-NB point8 [matrix]

For cumulative fit peak, R^2 = 0.99916

	Position	Height	Width	Area
peak1	1118	38.69	26.53	1569
peak2	1192	769.8	45.40	52941
peak3	1226	77.75	26.07	3216
peak4	1275	823.6	61.74	76575
peak5	1328	215.4	43.51	14321
peak6	1405	219.8	83.32	27354
peak7	1470	181.5	88.00	23817
peak8	1546	394.9	88.77	52138
peak9	1608	101.6	67.46	10321
peak10	1688	216.8	85.55	27353
peak11	1741	27.78	21.62	929.4

Figure S3.2 In sample S1-NB: (C) peaks were identified using a non-linear iterative curve fitting code used in Matlab ®. This code, ISignal, and other codes are completely free, available, and provided by Prof. T. O'Haver (University of Maryland, https://terpconnect.umd.edu/~toh/spectrum/). (D): peaks were identified by deconvolution using Lorentzian peaks in spectra (Origin©). Data were collected at *IFSC-USP* using wavelength of 785 nm, objective of 50x, acquisition time of 60 seconds, power ~ 0.35 mW, and a beam diameter of ~ 3μm.

S4. Carbon, hydrogen, and nitrogen elemental determinations

Table S4 reports average elemental abundances determined in intact samples. For each measurement, less than ~10 mg of powder was used permitting us to collect data on at least two sample's aliquots.

Table S4 CHN determinations.

Sample	C %	H %	N %	Total CHN (%)	Total second stage – TGA (%)
S51	0.17 (1)	0.03 (1)	0.02 (1)	0.22	0.23
S52	0.70 (4)	0.02 (1)	0.02 (1)	0.74	0.71
S1	0.36 (2)	0.40 (1)	0.03 (1)	0.79	1.67

Numbers in parenthesis represent uncertainty (1σ SD) in the last digits. Column Total second stage TGA from Table S8.

S5. FESEM images analysis

Figure S5.1 shows silica-1D particle size distributions (PSDs) calculated using constant size bins (25 nm) in Origin©. For these PSDs, input parameters were obtained via *ImageJ* processing of images in Figures 5 and 6, and Appendix C. PSDs show a peak size between 40 to 50 nm suggesting this such as a predominant particle's size. Particles up to ~500 nm in diameter were identified using this image processing.

For Figure 6, section 3.4, size versus circularity diagrams were calculated using constant size bins (25 nm for size, circularity was used in auto mode) in Origin© (3D diagrams not shown). Center of bins was used to plot size and average circularity. Power-law and decay exponential models were fitted in Origin©.
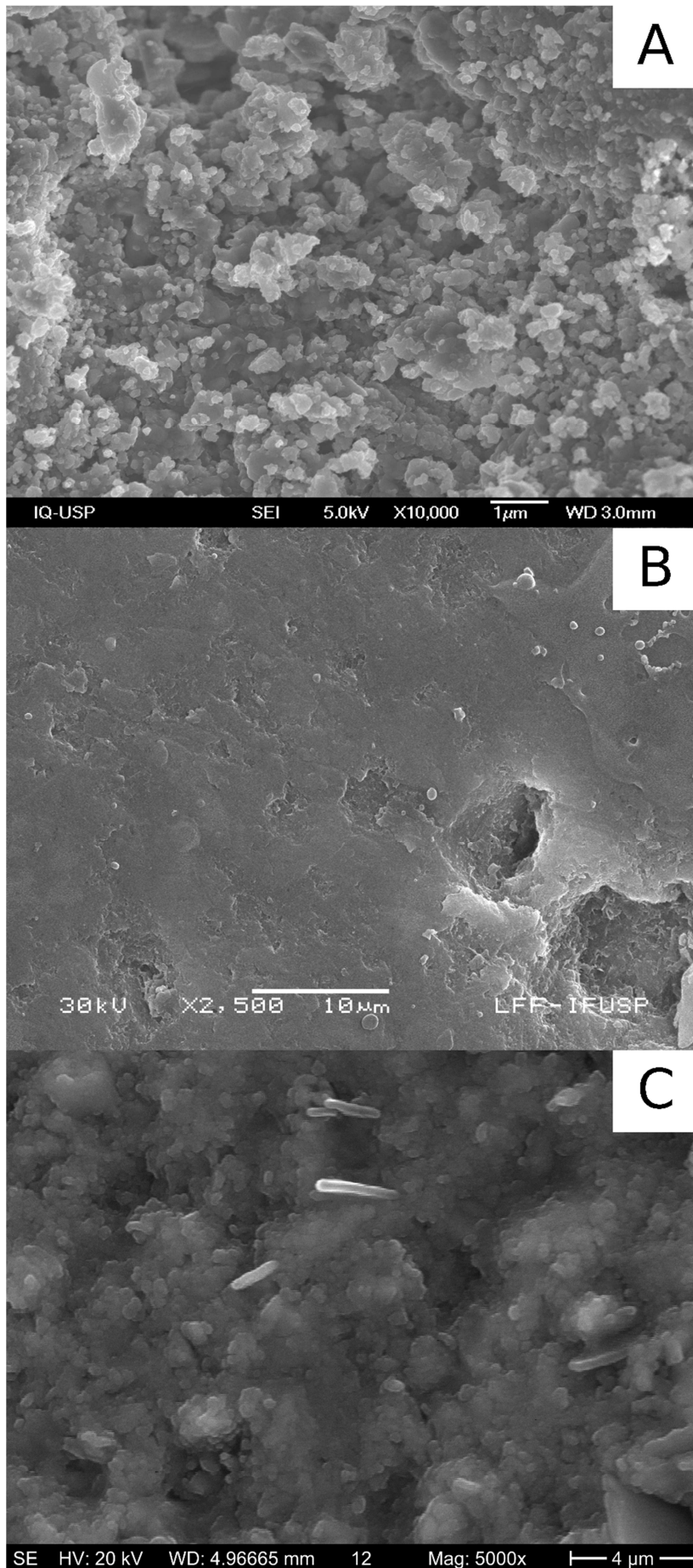
Figure S5.2 shows secondary electron images after different surface's preparation stages of sample S1. Better results were attained using HF-vapor etching followed by manual polishment. Samples S52 and S51 were prepared using this HF-vapor etching procedure. This method provided a clear visualization of chert's microstructure (Appendix C).

Figure S5.3 shows FESEM secondary electron images of combusted samples S1 and S51. These images were collected from fragments previously characterized by (U)SAXS. Previous to these FESEM experiments, etching of sample surfaces were performed using HF-vapor (~30 minutes) and then fragments were coated using a film of carbon of ~12 nm in thickness to ensure electrical conductivity.
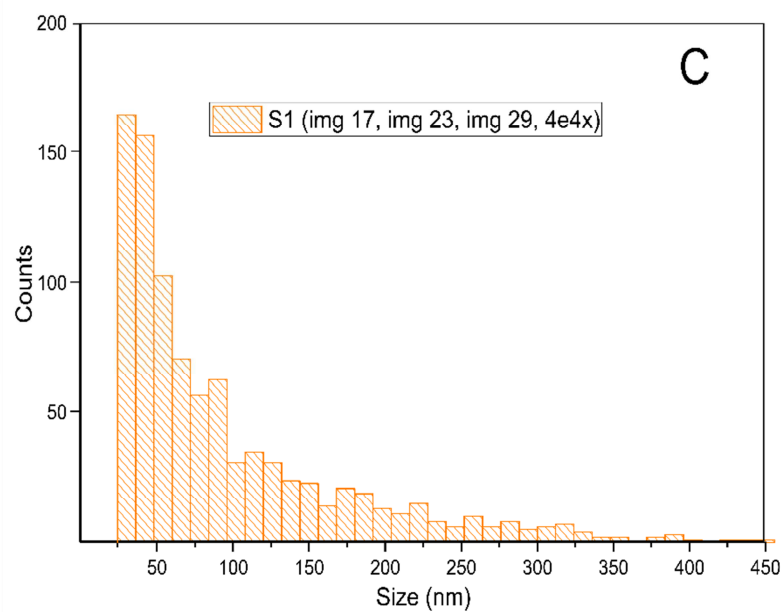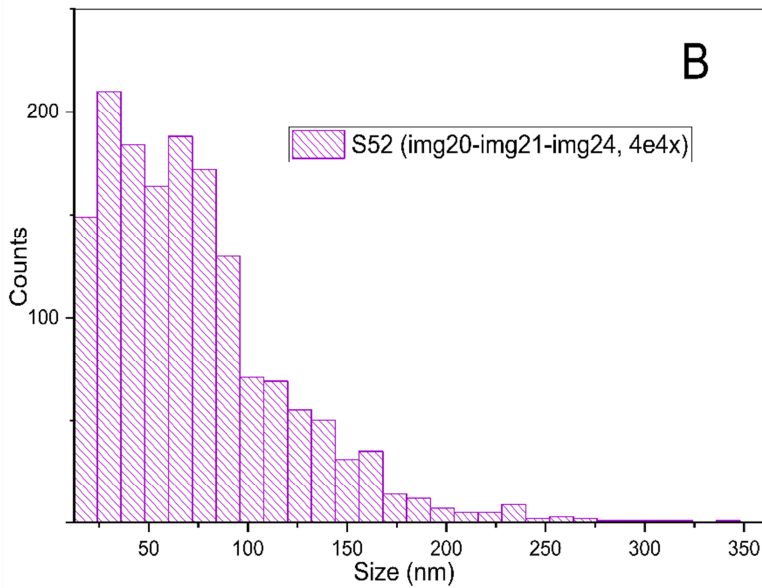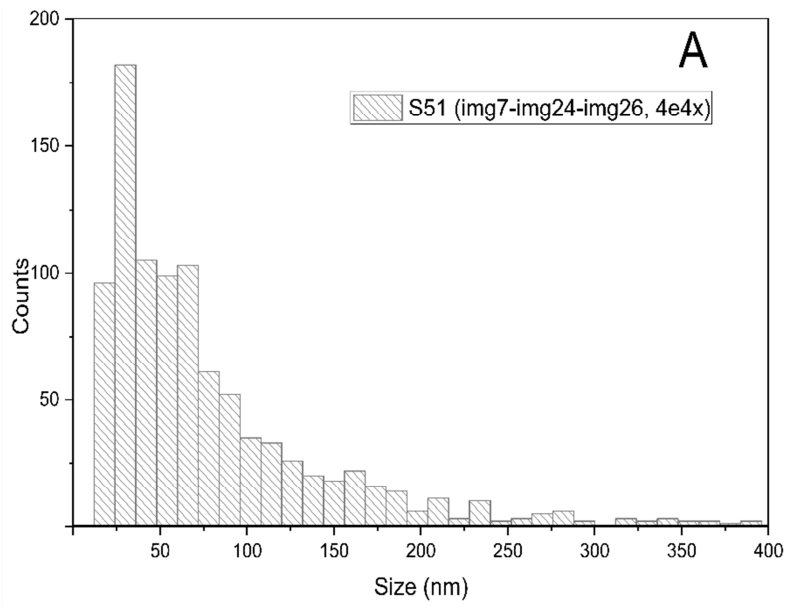
Figure S5.1 PSDs for intact samples. (A) sample S51, (B) sample S52, and (C) sample S1. Legend highlights the magnification and images used for analysis in *Image J*.

Figure S5.2 Secondary electron images depicting stages of S1 surface preparation. (A) HF-vapor etching + polishment, (B) polishment, (C) no treatment. Image A was collected at IQUSP. Image B was collected at *IFUSP*. Image C was collected at *IGc-USP*. Lower bars indicate analytical conditions.
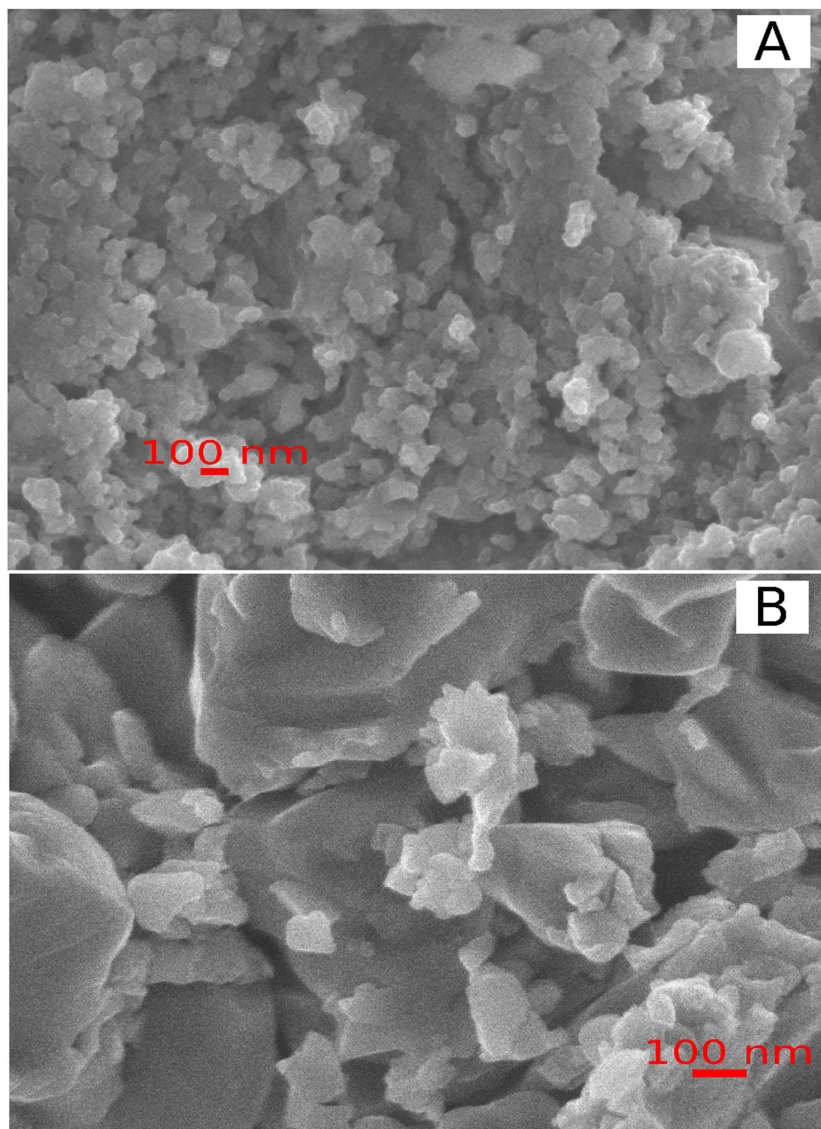
Figure S5.3 Secondary electron, FESEM images from samples S1 (A), S52 S51 (B). Both images were collected at magnifications of 40000X.

S6. N$_2$ adsorption-desorption isotherms

Figures S6.1 and S6.2 show some results for combusted samples. Intact samples not shown. Figure S6.1 displays adsorption (ads) and desorption curves (des). SSA and volume fraction values included in Table 1. Adsorption and desorption curves form hysteresis loops typically shown by mesoporous materials (Anovitz & Cole, 2015). Younger sample S1-B show a broad hysteresis loop. Older sample S51-B show a very narrow hysteresis loop, whereas S52-B exhibit a broader loop. Very narrow hysteresis loops are typical of materials with slit-like pores (Anovitz & Cole, 2015). FESEM images of sample S51 display this slit-shaped pores (Figure 5D).

Figure S6.2 shows pore size distribution (PSD) calculated from N$_2$ isotherms. Pore size indicated for these graphics differ significatively from those SAXS-based PVD (Figure 4). Also, total volume fractions estimated via N$_2$ isotherms are lower than porosities calculated from (U)SAXS data (Table 1). A large pore population was no probed by N$_2$ isotherm method. Also, these differences highlight (U)SAXS as almost the unique technique for a complete microstructural characterization of complex systems such as rocks.
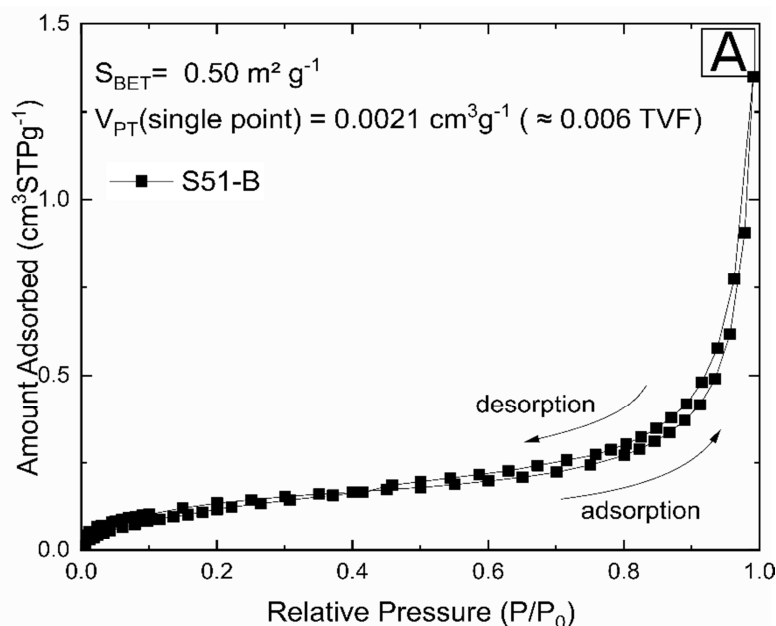
Figure S6.1 N_2 adsorption (ads) – desorption (des) isotherms for combusted samples. (A) sample S51-B, (B) sample S52-B, and (C) sample S1-B.
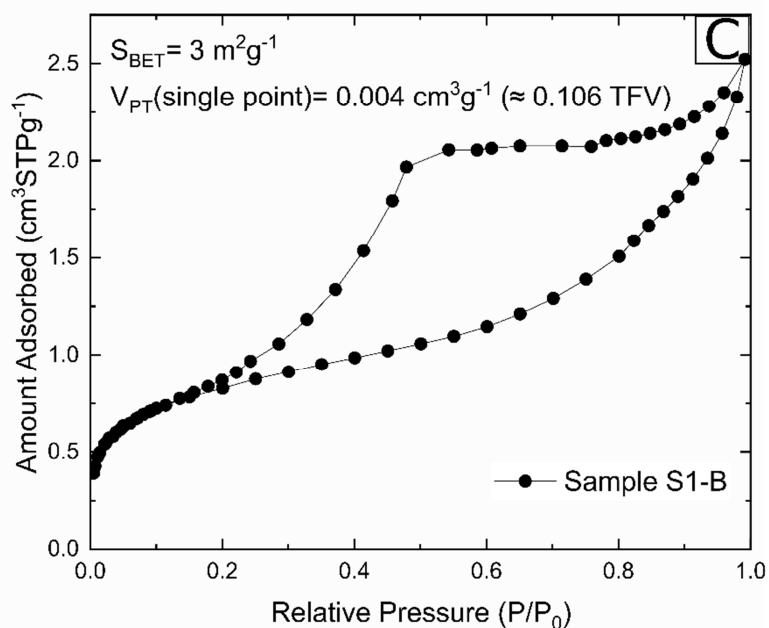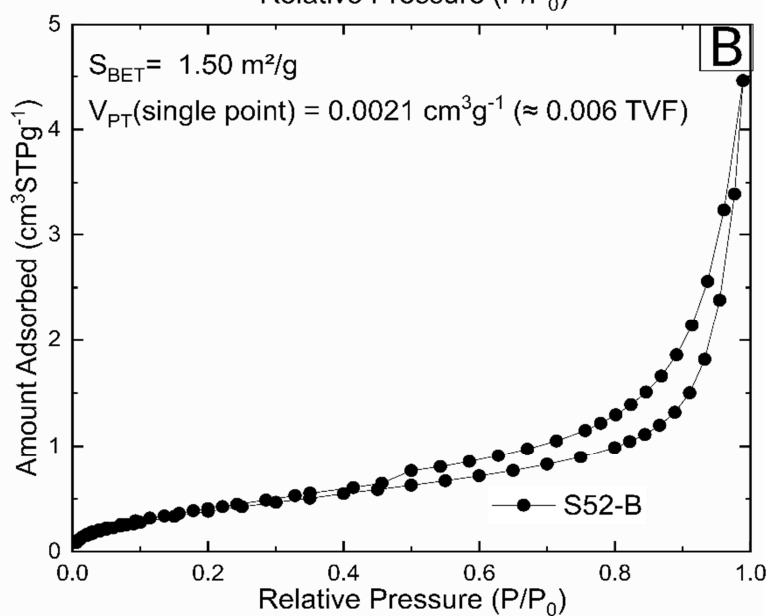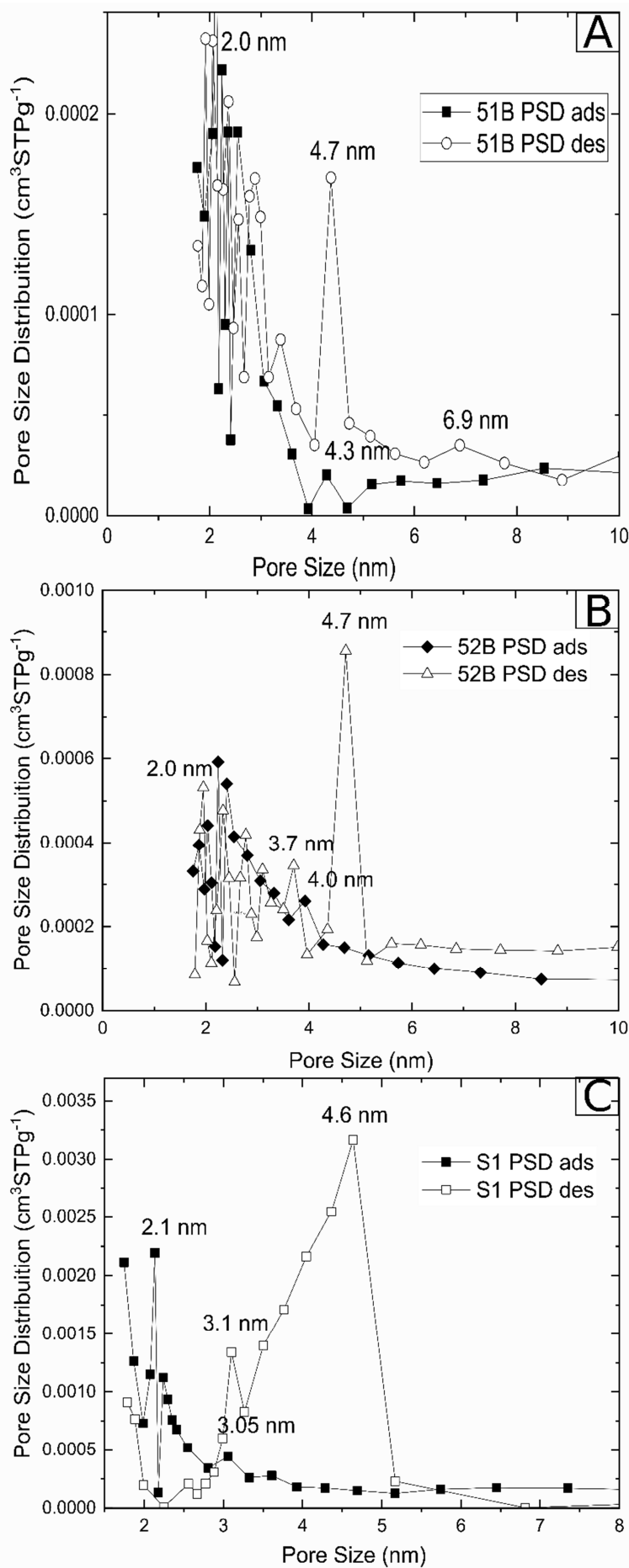
Figure S6.2 Pore Size Distribution (PSD) for combusted samples. (A) sample S51-B, (B) sample S52-B, and (C) sample S1-B.

S7. GC-FIC and GC-MS determinations

Table S7 shows occurrence of aliphatic and polycyclic aromatic hydrocarbons (PAHs) in part per billion. These low abundances are indicatives that carbon is mostly bonded in insoluble organic compounds (kerogen). This it is an expected result of time influence on organic matter despite its preservation inside porous matrix of chert.

Some PAHs represent biomarkers from different sources. Perylene has been reported to be derived from pigments of fungi (Whiteside & Grice, 2016). Meanwhile, pyrene has been reported such as a combustion-derived PAH (Whiteside & Grice, 2016).

Table S7   Quantification of aliphatic hydrocarbons and PAHs in intact samples (in $\mu g\ kg^{-1}$)

Aliphatic	Sample S1	Sample S52	Sample S51
C-12	<LD	<LD	<LD
C-13	<LD	<LD	<LD
C-14	<LD	432	598
C-15	<LD	<LD	<LD
C-16	5.83	<LD	413
C-17	2.73	<LD	<LD
Pristane	<LD	<LD	<LD
C-18	<LD	<LD	384
Phytane	<LD	<LD	<LD
C-19	<LD	<LD	<LD
C-20	6.7	363	404
C-21	<LD	<LD	<LD
C-22	4.51	501	515
C-23	12.5	227	<LD
C-24	74.0	<LD	<LD
C-25	59.6	<LD	<LD
C-26	73.0	661	300

Table S7. Continuation

Aliphatic	Sample S1	Sample S52	Sample S51
C-27	76.9	<LD	<LD
C-28	77.7	<LD	<LD
C-29	75.9	<LD	<LD
C-30	60.2	<LD	<LD
C-31	40.6	<LD	<LD
C-32	26.5	<LD	<LD
C-33	14.8	<LD	<LD
C-34	5.78	<LD	<LD
C-35	6.92	<LD	<LD
Aliphatic total	*624*	*2183*	*2613*

PAHs	Sample S1	Sample S52	Sample S51
Naphthalene	0.90	20.7	<LD
2-Methylnaphthalene	0.16	<LD	<LD
1-Methylnaphthalene	0.10	<LD	<LD
Phenanthrene	0.27	16.0	<LD
C1- Phenanthrene-Anthracene	ND	10.5	<LD
Fluoranthene	ND	3.8	<LD
Pyrene	0.08	1.6	<LD
Perylene	1.10	<LD	<LD
PAHs total	*2.61*	*52.6*	*0.0*

<LD: below detection limits. ND: non detected.

S8. TGA determinations

Table S8 reports estimated values for parameters from these curves. First stage (temperature range from 25 up to 200 ºC) of TGA curves is related to moisture from water adsorbed onto samples. Second stage (temperature range from 25 up to 1000 ºC) is mostly related to volatiles species released by combustion. These volatiles species are organic molecules, water, and hydroxyl functional groups from silanol groups (see Raman spectra, GC-MS and C-H-N data for a more detailed discussion). In sample S1, total volatile released during second stage (1.67%) is ~2X times greater than total CHN abundances (see Table S4). This fact could be related to releasing of OH groups from silanol groups (Si-OH) in sample S1. Broad DSC peaks limits an adequate estimation of dehydration heat in samples. The TGA curves of the 51-NB and 52-NB samples above 600 ºC show a small increase in mass, which may be related to the oxidation of some metallic species present in the sample, such as iron and manganese. These results corroborate those reported in μXRF maps (Figures S2.A and S2.B).
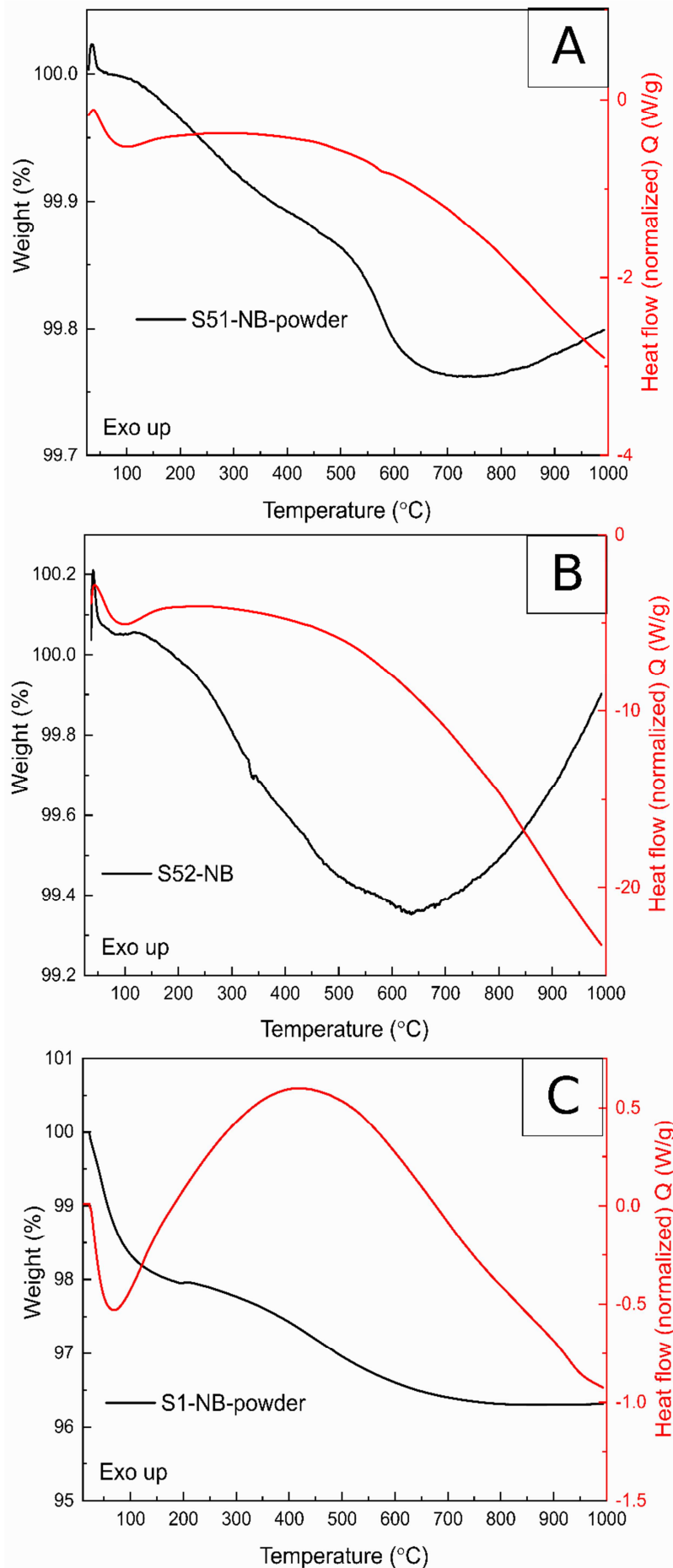
Figure S8 TGA (black) and DSC (red) curves collected in intact samples. (A) S51-NB, (B) S52-NB, and (C) S1-NB.

Table S8   Parameters estimated from DSC and TGA curves of Figure S8

Sample	First stage			Second stage		
	Δ mass (%) / [T range (ºC)]	T onset (ºC)	DSC (J/g) / [T peak (ºC)]	Δ mass (%) / [T range (ºC)]	T onset(ºC)	Residual mass (%)
51-NB-powder	**0.040** / [25-170]	-	131 [88]	**0.107** / [170-450] **0.115** / [450-760] 0.037* / [760-1000] *	206 533	99.8
52-NB-powder	**0.162** / [25-124]	-	597 [92]	**0.71** / [125-640] 0.53* / [640-1000] *	250	99.9
S1-NB-powder	**1.97** / [25-192]	41	266.3 [69]	**1.67** / [192-1000]	347	96.3

T: temperature. Δ mass: mass variation. T onset: extrapolated temperature corresponding to hydration or sample's degradation. T peak: Peak temperature in DSC curve. * Gain mass. In **bold** values used total volatile abundances reported in section 3.5.